Injection-depth-locking axial motion guided handheld micro-injector using CP-SSOCT

Gyeong Woo Cheon, Yong Huang, Hye Rin Kwag, Ki-Young Kim, Russell H. Taylor, Peter L. Gehlbach, and Jin U. Kang

***Abstract*— This paper presents a handheld micro-injector system using common-path swept source optical coherence tomography (CP-SSOCT) as a distal sensor with highly accurate injection-depth-locking. To achieve real-time, highly precise, and intuitive freehand control, the system used graphics processing unit (GPU) to process the oversampled OCT signal with high throughput and a smart customized motion monitoring control algorithm. A performance evaluation was conducted with 60-insertions and fluorescein dye injection tests to show how accurately the system can guide the needle and lock to the target depth. The evaluation tests show our system can guide the injection needle into the desired depth with 4.12µm average deviation error while injecting 50nl of fluorescein dye.**

I. Introduction

It is nearly impossible to perform micron-scale-precision tasks in freehand microsurgery even for highly-experienced surgeons. The main causes are target motion and hand tremor which exists mainly in the 6–12Hz frequency domain with 100µm of amplitude [1]. There have been several researches to address such motion problems actively [2-5]. For these reasons, we have been focusing on a simple axial motion compensation approach that utilizes optical coherence tomography (OCT) as a distal sensor that is combined with a linear motor [6-11]. As a distal sensor, common path OCT (CP-OCT) was chosen due to its simple structure and dispersion and polarization free characteristics [12-13]. In this paper, we introduce a freehand micro-injector that allows the injector tip to lock the desired depth during the injection with several micron order accuracy. To the best our knowledge, no micro-injector has been presented to meet such performance. To achieve this goal, we developed the control algorithm to expand the concept of motion control from passive position locking motion compensation to active position guidance to achieve highly precise injection-depth-locking. Depth targeting with high accuracy on the order of several microns is demonstrated with high repeatability. The potential effectiveness of precise drug delivery is also demonstrated.

This research supported by the U.S. National Institutes of Health and the National Eye Institute (NIH/NEI) Grant R01EY021540-01

G. W. Cheon, Y. Huang and J. U. Kang are with the Department of Electrical and Computer Engineering, Johns Hopkins University, Baltimore, MD, USA (e-mail: gcheon1@jhu.edu, yhuang60@jhu.edu, jkang@jhu.edu).

H. R. Kwag, is with the Department of Chemical and Biomolecular Engineering, Johns Hopkins University, Baltimore, MD, USA (e-mail: hkwag@jhu.edu).

K. Y. Kim, is with the Laboratory of Computational Sensing and Robotics, Johns Hopkins University, Baltimore, MD, USA (e-mail: kiyoung@kaist.ac.kr).

R. H. Taylor is with the Department of Computer Science, Johns Hopkins University, Baltimore, MD, USA (e-mail: rht@jhu.edu).

P. L. Gehlbach is with Wilmer Eye Institute, Johns Hopkins School of Medicine, Baltimore, MD (e-mail: pgelbach@jhu.edu).

II. Materials and Methods

A. System specification (Hardware)

The micro-injector system is comprised of three main modules: a handheld injector, a syringe-pump, and a main control module including a workstation, motor drivers, and a swept source OCT (SSOCT) based CP-OCT as shown in Fig. 1. The handheld injector uses a piezoelectric linear motor (LEGS-LL1011A, PiezoMotor), a tube-needle connector (RN Coupler-p/n 55752-01, Hamilton) that links a tube to a 34 gauge needle (Hamilton, OD=0.1842mm, ID=0.0826mm) inside a 26 gauge (OD=0.4636mm, ID=0.260mm) needle as a guide, and a fiber optic CP-OCT distal sensor probe. The injector housing was made by a 3D printing machine as shown in Fig. 2. The syringe-pump module is composed of a 100µl capacity syringe (Hamilton) with 1.46mm inner barrel diameter and 0.60mm-forward-push which corresponds to 1µl-volume-injection. A 1µm-precision linear actuator (850G Actuator, Newport) was used to accurately drive the syringe. To connect the injection needle remotely from the syringe, we used a 1m length of 1/16 inch PEEK tube (Tub PEEK Blu, IDEX). Prior to injection, all air bubbles were removed from all pathways. The main control module was used to process data and control the other modules.

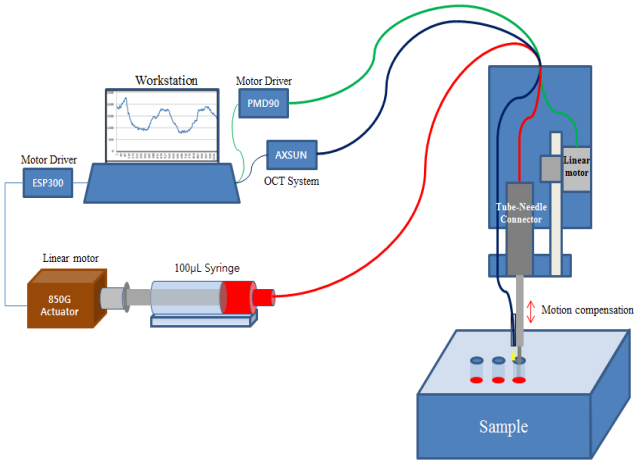

Figure 1. Overview of the micro-injector system.

The CP-OCT consists of a swept source OEM engine (AXSUN, central wavelength λ_0: 1060nm, sweeping rate: 100kHz, 3dB axial resolution: 8µm, scan range: 3.7mm in

air), a photo-detector and a digitizer with a sampling rate of up to 500 MSPS with 12 bit resolution, a Camera Link DAQ Board, and a Camera Link frame grabber (National Instruments). The sampled spectral data were processed using a quad-core workstation (Dell, Precision T7500) with GPGPU (GeForce GTX590, Nvidia). Two motor drivers were used: one for the piezoelectric linear motor in handheld injector module connected through a USB cable, which supports rapid response time, and the other driver to control the linear motor for syringe pump and a RS232 connection was used.

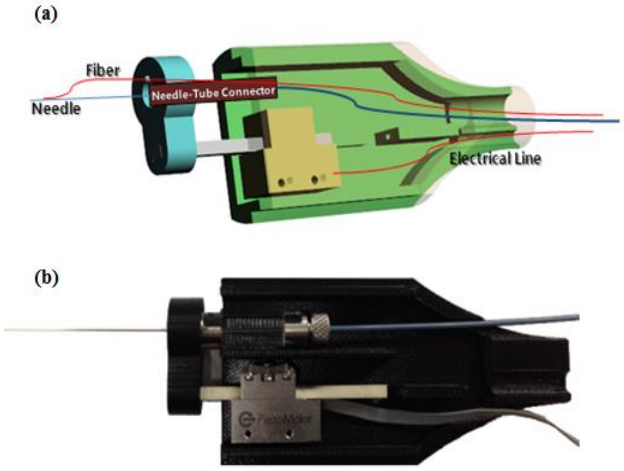

Figure 2. (a) CAD cross-sectional image of handheld micro-injector holder. (b) Photo image of the implemented handheld micro-injector.

B. *System specification (Software)*

The main goal in developing the control software was to ensure that freehand control is intuitive, real-time and highly precise. For a better response to hand tremor, the system oversampled and processed the OCT signal. One of the main control issues came from the inconsistent communication delay between the workstation and motor driver due to data buffering in the USB communications. To increase responsiveness, the minimum permissible value (= 2ms) was applied for maximum USB buffering time. However a 2ms delay in the critical path may still affect system performance. In consideration of the above mentioned limitations, all the processing was conducted and finished within that predetermined time frame.

In our setup, the workstation retrieves a buffered 128 spectral data from frame grabber in every 1.33ms. This value corresponds to 752 Hz response rate but the actual value varied in each instance depending on the delay time between the motor driver and the workstation. If the previous motor control command could not be executed before the next command arrived, then the prior command was abandoned and the driver executes the most recent command. The CP-OCT distal sensor data processing is similar to that of typical OCT image processing step except for the peak detection and the distal measurements between the sensor tip and the target. The sampled spectrum data (1376 data points) was averaged using 4 data sets to increase signal-to-noise ratio (SNR). Zero padding was conducted to increase the data points to 2048. Then, the spectrum sets were transformed to A-scan lines using a GPU based FFT (CUDA, Nvidia). The physical distance corresponds to one pixel is 3.6μm. For peak detection, second order Butterworth low-pass filtering was applied and was followed by peak detection to measure the distance between the fiber sensor tip and the target surface. Finally, the system sent a command to the motor driver to move the needle to a specific position at a specific velocity.

Fig. 3 shows the basic control algorithm of the system. The system has three conceptual states based on the distance between the tip of fiber and the surface of the sample. The states are 1) Free hand state, 2) Lock-in state, and 3) Stationary state. In free hand state, the system only observes the distance. Then, the injector motion is locked in and the needle tip is guided to the target depth by the system if the tip of injector passes over the lock-in boundary. Once the needle tip approaches the safety barrier (= target depth), the system tries to maintain the current position. After injection is done, the system automatically recognizes the user's pulling back or reset intention by monitoring the continuous fallback motion.

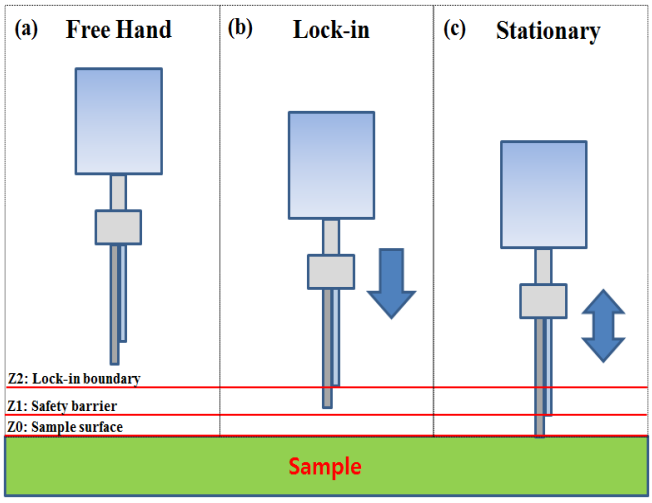

Figure 3. Three system states. (a) Free hand, (b) Lock-in, and (c) Stationary state. Each state is decided by the distance from the surface of sample.

C. *Experiment setup*

We used 10% gelatin samples shown in Fig. 4(b) to evaluate the micro-injector system. The gelatin was selected because it is very commonly used material in animal models and a wide range of hardness can be achievable by controlling the concentration of gelatin. Additionally, the transparent optical properties are advantageous in that the actual point of injection is directly observed from the side. First, we conducted needle insertion experiments to demonstrate how accurately the system can guide the needle and lock onto the target depth. A total of 60 insertions were carried out in the experiment. Next, we injected fluorescein dye, which has an absorption peak at 494 nm and an emission peak at 521 nm, to visualize the entire injection process.

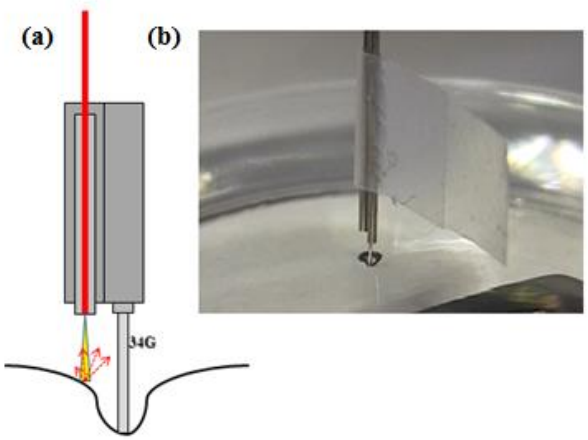

Figure 4. Surface deformation. (a) Conceptual image to show the passage of the reflected light in the deformation. (b) The actual deformation image in gelatin sample.

III. Results and Discussions

Before discussing the experimental result further, it is necessary to consider the issue of surface deformation caused by the needle at the time of insertion into the model gel used in this work. This is the result of the surface tension of the gelatin at the onset of needle penetration through the gel surface. This deformation problem prevents the OCT probe from receiving a proper distal signal from the sample surface as shown Fig. 4(a). Thus, the OCT distal sensor experiences a blind state during the insertion process with a 10% gel that may not be present with higher water content biological tissues, such as vitreous or retina.

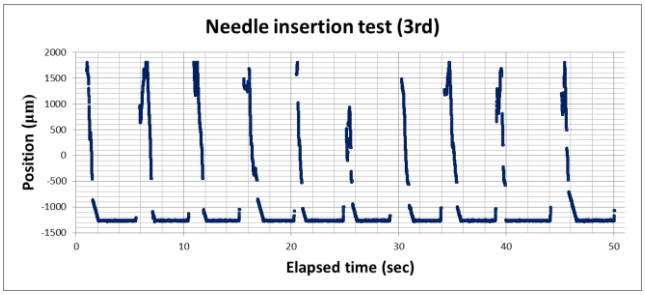

Figure 5. The third data consists of 60 insertions to show the OCT distal sensor signal variations during the injection process.

A. Insertion test

The insertion test was carried out in the following manner. The test involved 10 data sets and each data set consisted of 10 insertion trials. Fig. 5 shows the representative 3rd insertion data set. As mentioned previously, there was a "blind" zone around -500 microns to -1000 microns due to initial surface deformation in stiff gels. The size of the blind area can vary according to the sharpness and roughness of the needle tip, insertion speed and angle of insertion, etc. [14]. In our case, the insertion speed and angle were the main factors determining the range of the blind zone. Note that in this work we used a blunt tip needle and we expect that the surface deformation will be minimized by using sharp, smooth, bevel tipped needles of smaller gauge. Once the distal sensor signal is locked onto the boundary, the system guides the needle to the programmed target depth. The system maintains the locked position once the needle tip reaches the target depth. This is maintained until the tool senses the user pulling the needle out which is determined by the accumulated compensation length exceeding the compensating threshold or when the system loses the OCT signal continuously for greater than the preset fail count. Fig. 6 and Table 1 show the result of 60 insertions. The total average deviation error in injection state was 4.120µm

TABLE I. Average Deviation Error in Target Depth (Unit: Micron)

Data set	1st	2nd	3rd	4th	5th	6th
1	4.815	3.413	3.221	3.364	3.626	5.643
2	4.643	3.779	4.631	3.458	4.707	3.841
3	4.874	3.500	4.026	4.998	4.318	4.582
4	4.312	3.287	3.742	4.397	4.601	4.508
5	3.545	3.516	3.934	3.827	4.725	4.148
6	4.53	4.193	4.023	4.296	3.910	3.724
7	5.643	3.565	3.338	3.787	4.105	4.189
8	4.452	3.860	3.121	4.310	6.200	4.927
9	4.251	3.265	3.54	3.699	3.857	5.082
10	4.271	3.927	3.589	3.763	3.945	3.863
AVG	**4.534**	**3.631**	**3.717**	**3.990**	**4.399**	**4.451**

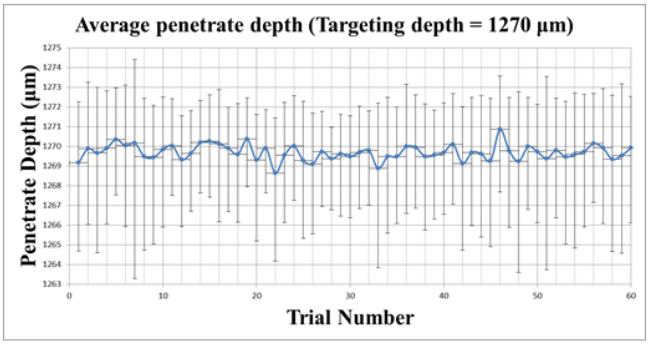

Figure 6. The average deviation error of 60 insertions with error bar consisted of standard deviation of positive and negative error.

B. Injection test

In the next set of tests, fluorescein dye was injected five times consecutively at a target depth. The blind zone still existed due to the surface deformation however the needle tip was still able to guide to the tip to the desired depth. The injection volume per injection was 50nl. Before injection, the system wait 1 sec to ensure the needle tip has properly locked onto the target depth. To inform the user of tool actions, an auditory signal was provided during the injection. As shown

Fig. 7(a) and 7(b), the fluorescein dye was injected to the target depth with average deviation error smaller than 5µm. As the dye was diffuses in gelatin, the injected droplet showed visible evidence of diffusion after a few seconds shown as Fig. 7(b)

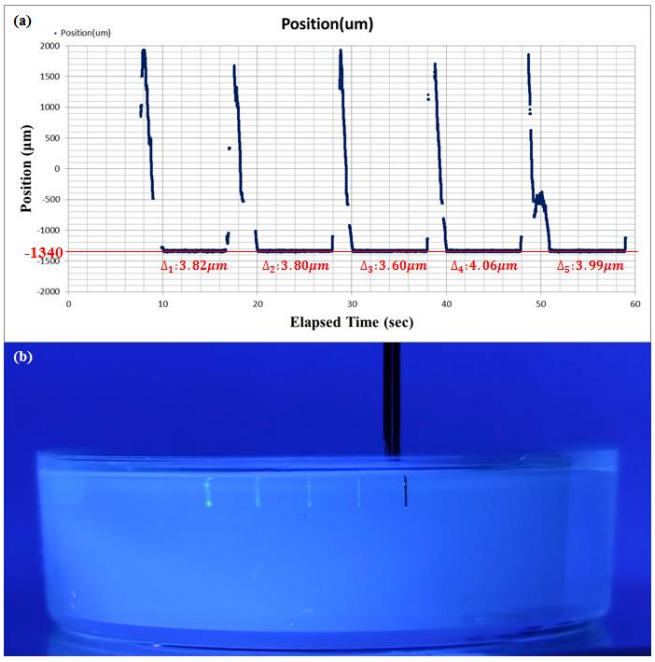

Figure 7. Consecutive 5 times fluorescein dye injection test. (a) Distance variation graph. (b) Photo image to show the injection.

IV. Conclusion

A handheld micro-injector system with highly accurate depth targeting capacity was developed and tested *in vitro*. A performance evaluation was conducted with multiple sets of insertion and fluorescein dye injection tests. The experimental results demonstrated that our micro-injector system can successfully compensated for hand tremor and guide a needle to deliver a test agent, in this case fluorescein to a desired depth with high precision (less than 5 micron). It automatically monitors user motion to initiate, guide, and reset the injector. Auditory feedback provides further control information for user.

Acknowledgment

The authors would like to thank to Sathappan Rameses for the help of using 3D printer for injector housing.

References

[1] S. P. N. singh and C. N. Riviere, "Physiological Tremor Amplitude during Retinal Microsurgery," in *Proceedings of the IEEE 28th Annual Northeast Bioengineering Conference, 2002*, IEEE, 2002, pp. 171–172.

[2] C. N. Riviere, J. Grangloff, and M. Mathelin, "Robotic Compensation of Biological Motion to Enhance Surgical Accuracy," in *Proceedings of the IEEE*, vol. 94(9), IEEE, 2006, pp. 1705–1716.

[3] R. Taylor, P. Jensen, L. Whitcomb, A Barnes, R. Kumar, D. Stoianovici, P. Gupta, Z. Wang, E. de Juan, Jr., and L. Kavoussi, "A steady-hand robotic system for microsurgical augmentation," in *Int. J. Robot. Res.*, vol. 18(12), IJRR, 1999, pp. 1201–1210.

[4] R. A. MacLachlan, B. C. Becker, J. Cuevas Tabares, G. W. Podnar, L. A. Lobes, Jr., and C. N. Riviere, "Micron: an actively stabilized handheld tool for microsurgery," IEEE Trans. Robot. vol. 28(1), 2012, pp. 195–212.

[5] J. Y. Ha, M. Shishkov, M. Colice, W. Y. Oh, H. Yoo, L. Liu, G. J. Tearney, and B. E. Bouma, "Compensation of motion artifacts in catheter-based optical frequency domain imaging," Opt. Express vol. 18(11), 2010, pp. 11418–11427.

[6] K. Zhang and J. U. Kang, "Common-path low-coherence interferometry fiber-optic sensor guided microincision," J. Biomed. Opt. vol. 16(9), 2011, 095003.

[7] K. Zhang, W. Wang, J. H. Hand , and J. U. Kang, "A surface topology and motion compensation system for microsurgery guidance and intervention based on common-path optical coherence tomography," IEEE Trans. Biomed. Eng. vol. 56(9), 2009, pp. 2318–2321.

[8] Y. Huang, K. Zhang, C. Lin, and J. U. Kang, "Motion compensated fiber-optic confocal microscope based on a common-path optical coherence tomography distance sensor," Opt. Eng. vol. 50(8), 2011, 083201.

[9] C. Song, P. L. Gehlbach, and J. U. Kang, "Active tremor cancellation by a "smart" handheld vitreoretinal microsurgical tool using swept source optical coherence tomography," Opt. Express, vol. 20(21), 2012, pp. 23414–23421.

[10] C. Song, D. Y. Park, P. L. Gehlbach, D. J. Park, and J. U. Kang, "Fiber-optic OCT sensor guided "SMART" micro-forceps for microsurgery," Biomed. Opt. Express, vol. 4(7), 2013, pp. 1045–1050.

[11] Y. Huang, X. Liu, C. Song, and J. U. Kang, "Motion-compensated hand-held common-path Fourier-domain optical coherence tomography probe for image-guided intervention," Biomed. Opt. Express, vol. 3(12), 2012, pp. 3105–3118.

[12] A. B. Vakhtin, D. J. Kane, W. R. Wood, and K. A. Peterson, "Common-path interferometer for frequency-domain optical coherence tomography," Appl. Opt., vol. 42(34), 2003, pp. 6953–6958.

[13] J. U. Kang, J. H. Han, X. Liu, and K. Zhang, "Common-path optical coherence tomography for biomedical imaging and sensing," J. Opt. Soc. Korea, vol. 14(1), 2010, pp. 1–13.

[14] A. M. Okamura, C. Simone, and M. D. O'Leary, "Force Modeling for Needle Insertion Into Soft Tissue," IEEE Trans. Bio. Eng. vol. 51(10), 2004, pp. 1707–1716.